Characterization of Devices, Circuits, and High-Temperature Superconductor Transmission Lines By Electro-Optic Testing

Final Technical Report

Principle Investigator:
John F. Whitaker
Assistant Research Scientist

Award Period:
1/15/89 - 1/14/91

Grantee:
University of Michigan
Ultrafast Science Laboratory
2200 Bonisteel, 1006 IST
Ann Arbor, MI 48109-2099

Grant No.:
NCC3-130

I. Introduction

The overall goal of this entire project, which has spanned two years, was to develop a capability for the testing of transmission lines, devices and circuits using the optically-based technique of electro-optic sampling. The ultimate achievement of this effort was the demonstration of electro-optic network analysis (*i.e.*, the extraction of all four *S*-parameters) of a high-speed device. The project has involved research on all of the facets necessary in order to realize this result, including the discovery of the optimum electronic pulse source, development of an adequate test fixture, improvement of the electro-optic probe tip, and identification of a device which responded at high frequency but did not oscillate in the test fixture.

In addition, during the process of investigating patterned high-critical-temperature superconductors, several novel, non-contacting techniques for the determination of the transport properties of high-T_c films were developed and implemented. These are a transient, optical pump-probe, time-resolved reflectivity experiment, an impulsive-stimulated Raman scattering experiment, and a terahertz-beam coherent-spectroscopy experiment. The latter technique has enabled us to measure both the complex refractive index of an MgO substrate used for high-T_c films and the complex conductivity of a $YBa_2Cu_3O_{7-x}$ sample. This information has been acquired across an extremely wide frequency range - from the microwave to the submillimeter-wave regime. The experiments on the YBCO were conducted without patterning of or contact to the thin film, thus eliminating the need for the more difficult transmission-line experiments.

Progress in all of these areas has been made and is documented in a number of papers which acknowledge the support of NASA Lewis. These papers may be found in the section listing the abstracts of the publications that have been issued during the course of this research.

II. Electrical Signal Source

The means of excitation for the device under test (DUT) in optically-based, broadband measurement systems are critical to the accuracy and usefulness of the *S*-parameters extracted. The most common means of generating an input for a device which is to be measured over a broad spectrum is to use a dc-biased photoconductive switch element. A standard Cr:GaAs photoconductive substrate produces a step output (on a picosecond time scale) when excited by a subpicosecond optical pulse, and it is not possible to use this type of signal for network analysis. This is due to the length of the pulse and the fact that reflected signals will be superimposed upon the input step, rendering it impossible to accurately resolve both the input to and any reflections from a DUT. This must be done in order to obtain the input and output reflection coefficients (S_{11} and S_{22}). We have

therefore had to investigate the implementation of materials such as radiation damaged silicon-on-sapphire (SOS) and low-growth-temperature epitaxial (LT) GaAs. These exhibit rapid, subpicosecond recombination of photoexcited carriers, generating short pulses which are easily transformed via Fourier techniques. Previous work with NASA Lewis Research Center involved the excitation of analog circuits with a step-like transient, and only qualitative results could be obtained in this instance. The generation of electrical *pulses* has allowed a complete quantitative analysis to be undertaken for device characterization.

In our investigation of material systems that would allow short-pulse generation, the carrier lifetime of GaAs was observed to decrease dramatically when grown by molecular beam epitaxy at very low substrate temperatures. For GaAs grown at ~200°C, 0.6-ps full-width-half-maximum electrical signals have been generated via photoconductive switching and measured by both electro-optic and photoconductive sampling (Fig. 1). Good responsivity is observed, especially compared to radiation-damaged SOS; a mobility value of ~120-150 $cm^2/V\text{-}s$ is determined for the photogenerated carriers. The material, when post-annealed, is also semi-insulating. The combination of the above properties makes it an ideal material for the photoconductive pulse generation needed for device testing.

III. Test Fixture

Waveforms which propagate on transmission lines or traverse the interconnections of integrated circuits can be readily measured via electro-optic sampling. While this is accomplished by immersing a probe tip into fringing electric fields, as shown in Fig. 2, it is somewhat more complicated to measure the response of a discrete device. This is because the device must be mounted in some sort of test fixture, as is the case for conventional, rf network analysis (such as that employing the HP8510 network analyzer). The test fixture must provide for the gate and drain dc biases; it must allow an input ac signal to be applied to the gate or drain side of the device; it must not have discontinuities that would cause reflections to appear on the measured waveforms (*i.e.*, impedances are matched); and it must be compatible with both electro-optic and rf measurement techniques so that a comparison can be made between the two techniques.

A test fixture which partially satisfied these conditions was designed and fabricated by engineers at NASA Lewis and the University of Michigan. NASA Lewis also procured a pseudomorphic High-Electron-Mobility Transistor (HEMT) from Hughes Research Laboratory that was secured in the microstrip test fixture and electrically connected via wire bonds.

Several important constraints on the microstrip test fixture were identified during the attempts that were made to measure the response of the Hughes HEMT device. The first was discovered during dc current-voltage measurements on the device bonded in the test fixture. This involved

instabilities in the I-V trace that were identified as oscillations. Despite the introduction of inductors, capacitors, or ferrite beads into the bias lines, the oscillatory behavior could only be diminished by a limited amount. Since it was possible that the oscillations might not have time to build up when the device input was a broad-bandwidth pulse, or that their existence might only appear as an input or output reflection coefficient greater than unity, it was decided to perform electro-optic measurements on the input and output ports of the device.

The discovery was thus made that there were several flaws in the design of this test fixture, one involving the positioning of the dc bias lines, the other arising from difficulties that are inherent to the nature of microstrip structures. Both of these problems lead to the same result: numerous reflected pulse signals appear along with the input pulse signal, obscuring the behavior of not only the input, but in particular the input reflected transient. An example of the mostly indecipherable waveforms acquired is shown in Fig. 3, where the voltage wave has been measured with an external electro-optic probe tip ~ 500 μm from the photoconductive switch and before the input port of the device. The part of the transient appearing earliest in the 40-ps window displays some of the characteristic behavior of modal dispersion, an effect expected on a transmission line with the large dimensions used (strip width = 180 μm; separation = 500 μm). These effects are an increased risetime, a decreased falltime, and ringing after the main body of the pulse (due to a phase velocity that decreases with increasing frequency). However, most of the ringing following the earliest pulse is due to multiple reflections from both the dc bias lines and the ground plane of the microstrip.

In order to verify that some reflections could indeed originate at the interface of the substrate and the ground plane, a comparison was made between pulses generated and measured on both microstrip and coplanar stripline (CPS). While the transient on the coplanar line consisted of a single pulse and then a flat baseline response, the signal on the microstrip demonstrated a periodic response of significant amplitude which followed in time behind the main pulse (Fig. 4). This is attributed to the ground plane, which is present in the microstrip sample but not in the coplanar one.

Since the reflections could not be eliminated using the original design, it was necessary to modify the test fixture. The result of the modification appears in Fig. 5. Since the coplanar stripline was proven to provide a superior environment for pulse generation and propagation, this structure was employed to transmit the input signals to the DUT. A gap embedded into the CPS served as the photoconductor switch, and an extension to one of the CPS conductors was used to provide dc bias to the DUT. Thus, both dc and broadband excitations were brought to the device without any intermediate discontinuities. The transient generated by the 100-fs laser pulses used in our experiments propagated down the CPS and served as the input stimuli to the DUT. The lines had 50-μm-wide conductors and a 5-mm-wide center gap, yielding a characteristic impedance of ~55 Ω. This geometry effectively eliminated transmission and bias-line discontinuities so that the test fixture

was not a limiting factor in making *S*-parameter measurements up to ~ 100 GHz.

IV. Electro-Optic Probe Tip

During the course of this research, it was also discovered that the dimensions of the electro-optic probe tip used to make transient measurements can exert a great influence on the waveforms obtained. Specifically, one probe-tip of a given thickness may not reproduce a voltage waveform as faithfully as a another tip with different thickness. To demonstrate this, several different tips were produced and used to test a pulse signal propagating on a coplanar stripline having conductors 30-μm wide separated by 20 μm. The tips consisted of a lithium tantalate ($LiTaO_3$) crystal mounted on a fused silica support. These units were polished to the same inverted, truncated-pyramid shape with an angle of ~25° to the normal of the base. In each case the table of the probe was positioned flat against the substrate and the conductors.

Figure 6 consists of (a) side and (b) cross-sectional views of the external electro-optic probe and coplanar strip transmission line geometries used in the experiment. Three interfaces created reflection sources that could direct part of the electrical signal back to the measurement point: (i) $LiTaO_3$ upper boundary and fused silica support; (ii) substrate bottom; (iii) output facet of $LiTaO_3$ crystal where the guided electrical signal re-enters the open-boundary part of the coplanar stripline. The reflection from interface (ii) is similar to the one described for microstrip lines described above, except that for the CPS without a ground plane, a material that absorbs or couples out the wave travelling to the bottom of the substrate can be attached to the interface. The reflection from interface (iii) also was found to be of minimal concern, as its amplitude appeared to be relatively small. Thus, the reflection with the greatest influence was found to originate at interface (i), and the tips compared were varied in thickness rather than face dimension.

The four probes used to make the measurements were polished to thicknesses of 500, 300, 100, and 20 μm. We expected the true signal output from the photoconductive switch to be a single-picosecond-duration electrical pulse. However, as can be seen in the results shown in Fig. 7, there was a long tail with pronounced ringing on the top three measured waveforms. The main ringing features were found to correspond to the $LiTaO_3$ crystal thickness and, as mentioned above, have been attributed to electromagnetic radiation coupling into the $LiTaO_3$ crystal and resonating between the top and bottom crystal interfaces. Indeed, the time it takes the signal to reach the fused-silica/$LiTaO_3$ interface and then return, given by

$$t_{rad} \approx 2d \frac{\sqrt{\varepsilon_r}}{c}$$

(where d is the $LiTaO_3$ crystal thickness, c the speed of radiation in vacuum, and ε_r the relative permittivity of $LiTaO_3$), predicted expected delays that matched the measured ones: ~ 4.4 ps vs. ~3.5 ps, respectively, for the 100-μm-thick crystal; 13 ps vs. ~13 ps for the 300-μm crystal; and 22 ps vs. ~22 ps for the 500-μm crystal. Thus, we attribute the main measurement error for this type of crystal to bulk resonant effects.

Since the sampling beam integrates the transverse-electric-field strength along its entire path in the $LiTaO_3$, the whole thickness of the crystal was found to affect the probe beam and the measured output. Thus, in addition to the main ripples observed on the signals, we also observed that the signal was generally corrupted throughout the measurement time window.

The best way found to eliminate the deleterious effects of the EEP material bulk was to employ a thin $LiTaO_3$ crystal that acted as a single lumped-element and eliminated the undesirable bulk resonant effects. The optimal thickness was expected to be similar to the extent of the guided mode confinement near the conductors. A thicker than optimum crystal would exhibit resonance, and a thinner one would have reduced sensitivity due to a reduced signal integration path. For typical microwave coplanar transmission lines with dimensions of 5 to 50 μm, an optimum crystal thickness was expected to be ~20 μm. The bottom trace of Fig. 7 shows the measured signal at the center of an ~20-μm-thick EEP with a 200 x 200-μm-footprint dimension. The long-lived ringing tail has disappeared, while the sensitivity remained practically unchanged.

V. *S*-Parameter Measurements

In order to perform two-port network analysis using external electro-optic sampling, the amplitude and phase of the input and output waves for a three-terminal device had to be measured. The HEMT devices which were ultimately analyzed were given to the University of Michigan by General Electric's Electronics Laboratory. It was decided to test these devices since the Hughes HEMTs were initially found to oscillate in the microstrip test fixture, and the GE staff was eager to collaborate, contributing rf *S*-parameter measurements on numerous devices.

Typical positions of the $LiTaO_3$ probe tip used to measure the voltage signals at the input and output of the DUT are indicated in Fig. 5. The probe would first be placed at the input side of the device in a position far enough from the switch or the device so that both the incident and reflected signals could be acquired (probe and sampling spot positions to the left of the DUT in Fig. 5). The probe tip would then be moved to the output port of the network to capture the transmitted transient (probe and spot positions to the right of the DUT).

Figure 8 consists of two time-domain plots of the waveforms measured at the input and output ports of the test fixture. As already described, when the switch on the gate side of the fixture was the one activated, the signal measured by the probe tip on this side contained both the incident and reflected waveforms. The signal measured on the drain side exhibits some positive capacitive feedthrough and then the inverted and amplified drain output. The voltage scales are in arbitrary units in this instance.

A comparison of the spectra of these waves, along with the waves measured when the input transient was connected to the drain side of the DUT, led to the determination of all four *S*-parameters of the HEMTs tested. The spectra were obtained through simple signal processing, namely algorithms running on a personal computer that perform a digital Fourier transform. For one 0.15-μm gate length AlGaAs HEMT, the *S*-parameters measured electro-optically to 100 GHz are displayed in Fig. 9 (dotted line). The solid lines give the *S*-parameters to 40 GHz, as measured via a conventional rf network analyzer. Except for S_{22}, the agreement between the measurements of the two techniques is excellent.

Comparisons were also made for two other HEMT devices, one AlGaAs and one InAlAs, with very good agreement again attained for both. Two measurements of the S_{21} for the latter device are shown in Fig. 10 (X for rf analysis; O for electro-optic). For each device, the two contrasting techniques were used to measure devices from the same wafer, and for both of the electro-optic and rf measurements the devices were connected to their respective test fixtures via wire bonds to the gate, drain, and source pads.

From electro-optic data such as that acquired in Fig. 10, one can make determinations of cutoff frequency that are not extrapolated from low-frequency rf measurements. That is, direct measurement of the device behavior is made possible.

VI. High-Critical-Temperature Superconductors

One of our goals has been to investigate the response of high-critical-temperature superconductors under broadband, millimeter-wave excitation. While the application of patterned films as transmission lines is one realistic way to accomplish this, it is also a difficult one due to the fact that the material has to be patterned, good contacts must also be made to it, and any results must have the influence of the guiding structure removed. These problems have been avoided through the use of a non-contacting, free-space radiation, terahertz-beam, spectroscopy technique.

One outstanding application of photoconductive elements, when they are fabricated on substrates with rapid recombination times, is as transmitting and receiving antennas that can be used for millimeter-wave and submillimeter-wave spectroscopy. This technique, which differs from single-frequency methods using cavities or resonators, has been used to study dielectrics and semiconductors in the millimeter-wave regime. Furthermore,

Fourier-transform infrared spectroscopy, which has been employed for characterization in the far-infrared regime, possesses inferior signal-to-noise properties compared to the time-domain measurements of the terahertz-beam system. The time-domain technique is also a coherent one, so that both phase and amplitude information are obtained directly from measurements.

When high-T_c materials are the samples measured by coherent time-domain spectroscopy, insight may be gained into the nature of quasiparticle excitations and pairing mechanisms, and one can also get a direct assessment of how the materials would perform as passive microwave devices such as interconnects, resonators and filters. This information is found via measurements of the transmission of terahertz beams through the high-T_c films and their substrates, from which the complex conductivity of the films may be determined.

A schematic of the system used is shown in Fig. 11. The 100-fs laser pulses triggered photoconductive gates in both the transmitter and the receiver, the latter element being used as a sampling gate. The photoconductive switch in the transmitter is located at the center of a simple dipole-like antenna imbedded in a coplanar transmission line. To aid the coupling of the radiation into the air and to provide collimation of the terahertz beam, a hyperhemispherical dome lens fabricated from high-resistivity silicon was placed at the back of the antenna substrate as shown. The terahertz beam was collected and focussed onto an identical receiving antenna, across which the electric field associated with the collected radiation induced a transient bias voltage. The amplitude and temporal profile of this induced voltage was obtained by measuring the collected charge versus the pump-probe delay time.

The temporal response for our system is shown in Fig. 12a. This was obtained by using low-temperature, MBE-grown GaAs for both the transmitting and receiving photoconductive gates. The central spike of the radiation burst has a full-width at half-maximum under 440 fs. The corresponding spectral magnitude obtained by directly applying a numerical fast Fourier transform is shown in Fig. 12b. There are frequency components which extend beyond 2.5 THz. By placing the sample under study between the transmitting and receiving antenna, the transmission function (*i.e.*, the frequency response measured with the sample between the antennas divided by the response without the sample) was obtained with both magnitude and phase information.

We first applied this technique to assess the characteristics of a MgO substrate on which the high-T_c thin films were later deposited. From a measurement of the transmission function, the complex index was directly obtained. The results are shown in Fig. 13. The real part of the index increased only slightly with frequency. Indeed this demonstrated the ability to accurately measure index changes of less than 1% over a bandwidth exceeding 2 THz in thin samples (0.5 mm). From the imaginary part of the index the absorption was found to be < 1 cm^{-1}. These properties made this

substrate an excellent choice to measure the transmission properties of high-T_c thin films.

Next a superconducting YBCO thin film (~1000-Å thickness) was placed between the antennas. The epitaxial *c*-axis oriented film was produced using a standard laser-ablation process at Eastman Kodak. Figure 14 shows the time-domain response in transmission for temperatures above and below the critical temperature (~80 K). The changes associated with the onset to superconductivity can be directly seen. A dramatic decrease in the transmitted signal amplitude occurred as a result of the increase in the reflection of the incident wave. An even more dramatic change can be seen for temperatures below ~ $T_c/2$. A phase shift and an accompanying change in pulse shape are also identified. This is a direct result of the presence of superconducting electrons.

By using similar techniques as those used for dielectrics, the complex index and conductivity were obtained directly from these measurements at frequencies approaching 2 THz. These are shown in Fig. 15. As expected, there is a large contribution to the conductivity below T_c due to superconducting electrons (σ_2), while there is no contribution to the conductivity from σ_2 at temperatures above T_c.

Abstracts of Published Material

• "External electro-optic probing of millimeter-wave integrated circuits," J.F. Whitaker, J.A. Valdmanis, T.A. Jackson, K.B. Bhasin, R. Romanofsky, and G.A. Mourou, *1989 IEEE MTT-S International Microwave Symposium Digest*, vol. 1, pp. 221-224 (1989).

Abstract: An external, non-contact electro-optic measurement system, designed to operate at the wafer level with conventional wafer probing equipment and without any special circuit preparation, has been developed. Measurements have demonstrated the system's ability to probe continuous and pulsed signals on microwave integrated circuits on arbitrary substrates with excellent spatial resolution. Experimental measurements on a variety of digital and analog circuits, including a GaAs selectively-doped heterostructure transistor prescalar, an NMOS silicon multiplexer, and a GaAs power amplifier MMIC are reported.

• "External electro-optic integrated circuit probing," J.F. Whitaker, J.A. Valdmanis, M.Y. Frankel, S. Gupta, J.M. Chwalek, and G.A. Mourou, *Microelectronic Engineering*, vol. 12, pp. 369-379 (1990). Also, presented as an invited talk at the Second European Conference on Electron and Optical Beam Testing of Integrated Circuits, Oct. 1-4, 1989, Duisburg, F.R.G.

Abstract: An external electro-optic measurement system with subpicosecond resolution has been developed. This electro-optic sampling system is designed to operate as a non-contact probe of voltages in electrical devices and circuits with modified wafer-level test equipment and no special circuit preparation. Measurements demonstrate the system's ability to probe continuous and pulsed signals on microwave integrated circuits on arbitrary substrates with single-micron spatial resolution. We also discuss the application of external electro-optic sampling to various aspects of time-domain circuit studies, including the generation of short electrical test pulses using novel photoconductive techniques and the propagation of pulses on interconnects.

• "100-GHz Electro-optic *S*-parameter characterization of high electron mobility transistors," M.Y. Frankel, J.F. Whitaker, G.A. Mourou, J.A. Valdmanis, and P.M. Smith, to be presented as an invited talk at the Picosecond Electronics and Optoelectronics Topical Meeting, March 13-15, 1991, Salt Lake City, Utah.

Abstract: We report the first use of external electrooptic sampling for the direct, non-extrapolated measurement of *S*-parameters for high-electron-mobility transistors over a bandwidth of 100 GHz.

• "Experimental characterization of external electro-optic probes," M.Y. Frankel, J.F. Whitaker, G.A. Mourou, and J.A. Valdmanis, *IEEE Microwave and Guided Wave Letters*, vol. 1, pp. 60-62 (Mar. 1991).

Abstract: The accuracy and invasiveness of various external $LiTaO_3$ electro-optic probe geometries is investigated experimentally. Such probes are an integral part of external electro-optic sampling systems used for the measurement of high bandwidth electrical signals in microwave integrated circuits. The experimental results indicate that for optimum measurement accuracy and minimum invasiveness of the probe, the electro-optic crystal should be no thicker than the extent of the microwave coplanar transmission line guided mode. Thinned crystals possess additional advantages of reduced thermal drift and reduced stray signal pickup from adjacent signal lines.

• "High-voltage picosecond photoconductor switch based on low-temperature-grown GaAs," M.Y. Frankel, J.F. Whitaker, G.A. Mourou, F.W. Smith, and A.R. Calawa, *IEEE Trans. on Electron Devices*, vol. 37, pp. 2493-2498 (Dec. 1990).

Abstract: A GaAs material grown by molecular beam epitaxy (MBE) at a low substrate temperature was used to fabricate a photoconductor switch that produces 6-V picosecond electrical pulses. This is the highest impulse voltage with a picosecond duration ever generated. The low-temperature (LT) GaAs is well suited for application to high-voltage picosecond switching, because it has a high dark resistivity, a high dielectric-breakdown strength, a subpicosecond carrier lifetime, and a high minority-carrier mobility. The pulses were produced on a microwave coplanar strip transmission line lithographically patterned on the LT GaAs. A 150-fs laser pulse was used to generate carriers in the LT GaAs gap between the metal strips, partially shorting a high dc voltage placed across the lines. The 6-V magnitude of the electrical pulses obtained is believed to be limited by the laser pulse power and not by the properties of the LT GaAs. Experiments were also performed on a picosecond photoconductor switch fabricated on a conventional ion-damaged silicon-on-sapphire substrate. Although comparable pulse durations were obtained, the highest pulse voltage achieved with the latter device was 0.6 V.

• "Low-temperature epitaxially-grown GaAs as a high-speed photoconductor for terahertz spectroscopy," J.M. Chwalek, J.F. Whitaker, and G.A. Mourou, to

be presented at the Picosecond Electronics and Optoelectronics Topical Meeting, March 13-15, 1991, Salt Lake City, Utah.

Abstract: Low-temperature epitaxially-grown GaAs layers with a 0.44 ps response time have been used for the photoconductive generation and detection of multiple-terahertz radiation bursts useful for spectroscopy.

• "Submillimeter-wave response of superconducting $YBa_2Cu_3O_{7-x}$ using coherent time domain spectroscopy," J.M. Chwalek, J.F. Whitaker, and G.A. Mourou, submitted to *Electronics Letters* (January 1991).

Abstract: A coherent time-domain technique utilizing freely propagating radiation bursts is used to study the submillimeter-wave response (extending to 1.4 THz) of an $YBa_2Cu_3O_{7-x}$ thin film above and below the critical temperature. From these measurements the complex dielectric response, and hence the complex conductivity, were directly obtained.

• "Femtosecond optical absorption studies of nonequilibrium electronic processes in high-T_c superconductors," J.M. Chwalek, C.Uher, J.F. Whitaker, G.A. Mourou, J. Agostinelli, and M. Lelental, *Appl. Phys. Lett.*, vol. 57, pp. 1696-1698 (Oct. 1990).

Abstract: We report the results of femtosecond optical transient absorption experiments performed on the superconducting compounds $YBa_2Cu_3O_{7-x}$ ($x \sim 0$) and $Bi_2Sr_2Ca_2Cu_3O_{10+\delta}$ ($\delta \sim 0$) and nonsuperconducting $YBa_2Cu_3O_{6+y}$ ($y < 0.4$) for sample temperatures ranging from ~ 7K to room temperature. Nonequilibrium heating was found to occur on a subpicosecond timescale. A distinct, dramatic increase in the relaxation time was observed for the superconducting samples as the sample temperature was lowered below the critical temperatures of the respective films. Accompanying the increase in relaxation time was an increase in the peak fractional transmissivity change. No such changes were observed for the nonsuperconducting YBCO sample. We believe the above described behavior is electronic in origin and intimately related to the superconductivity of the compounds.

• "Subpicosecond time-resolved studies of coherent phonon oscillations in thin-film $YBa_2Cu_3O_{6+x}$ ($x < 0.4$)," J.M. Chwalek, C.Uher, J.F. Whitaker, G.A. Mourou, and J. Agostinelli, to appear in *Appl. Phys. Lett.*, vol. 58 (Mar. 1991).

Abstract: We report the results of the first time-resolved observation of impulsively generated coherent optical phonon oscillations in the semiconducting cuprate compound $YBa_2Cu_3O_{6+x}$ ($x < 0.4$). The oscillations, which were probed through time-resolved transmissivity modulation, had a period of 237 fs at room temperature, corresponding to a Raman active mode

of A_{1g} symmetry at 142 cm^{-1}. No oscillations were observed in the superconducting form of Y-Ba-Cu-O either above or below T_c. The amplitude, frequency, and linewidth of this mode was measured over a temperature range from ~7 K to room temperature.

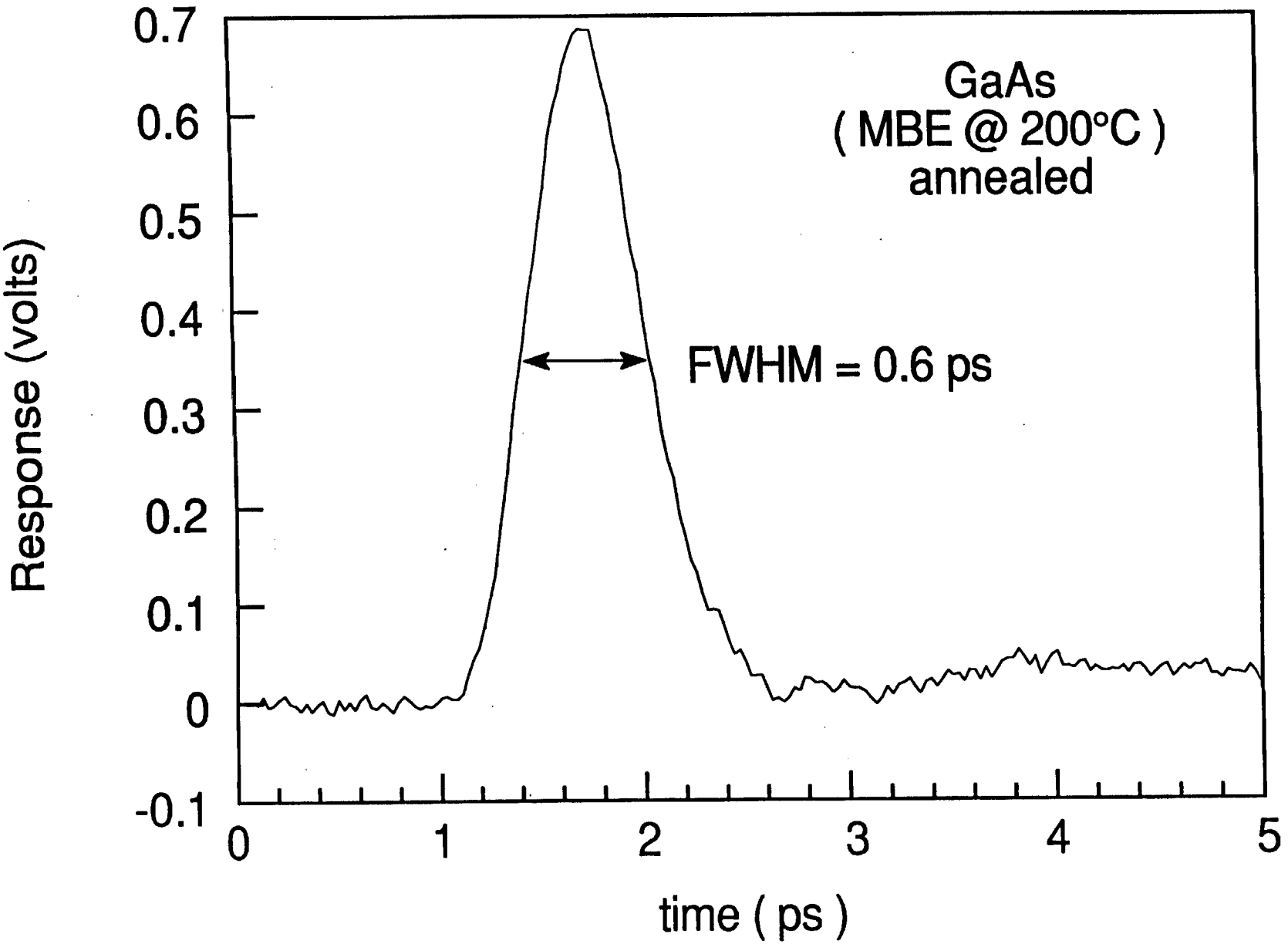
GaAs
(MBE @ 200°C)
annealed
FWHM = 0.6 ps
Response (volts)
time (ps)
0.7
0.6
0.5
0.4
0.3
0.2
0.1
0
-0.1
0
1
2
3
4
5

Fig. 1

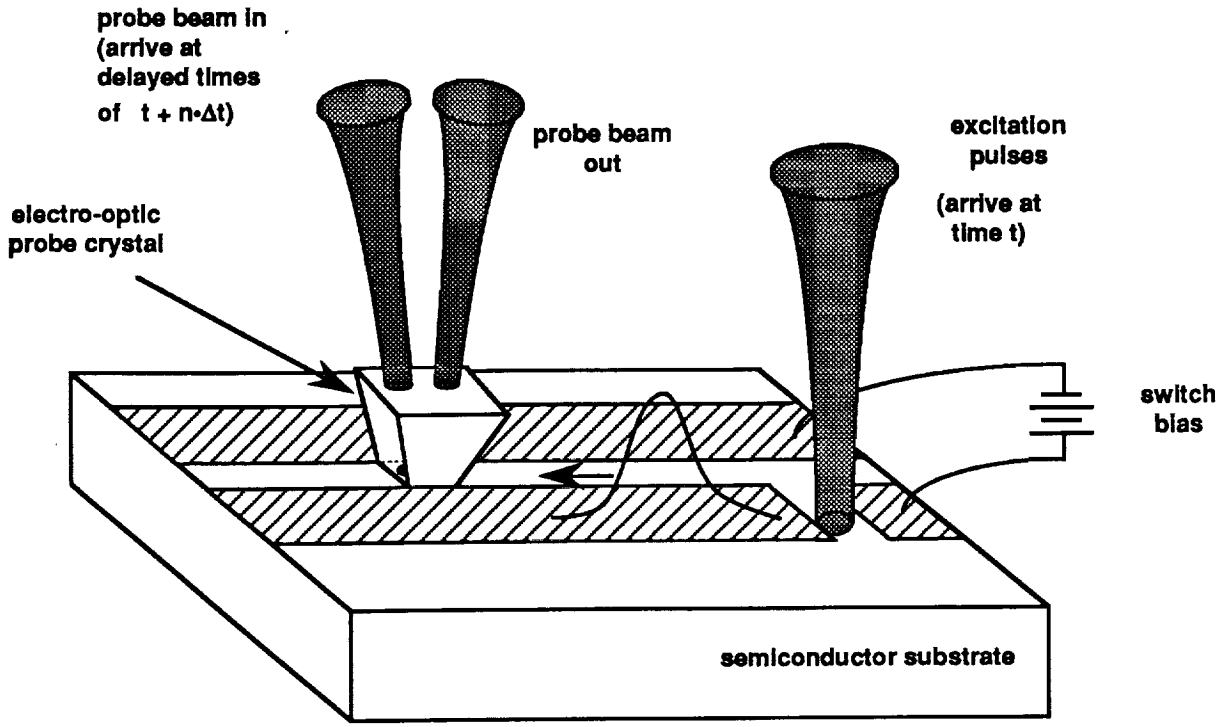
probe beam in
(arrive at
delayed times
of t + n•Δt)
probe beam
out
excitation
pulses
(arrive at
time t)
electro-optic
probe crystal
switch
bias
semiconductor substrate

Fig. 2(a)

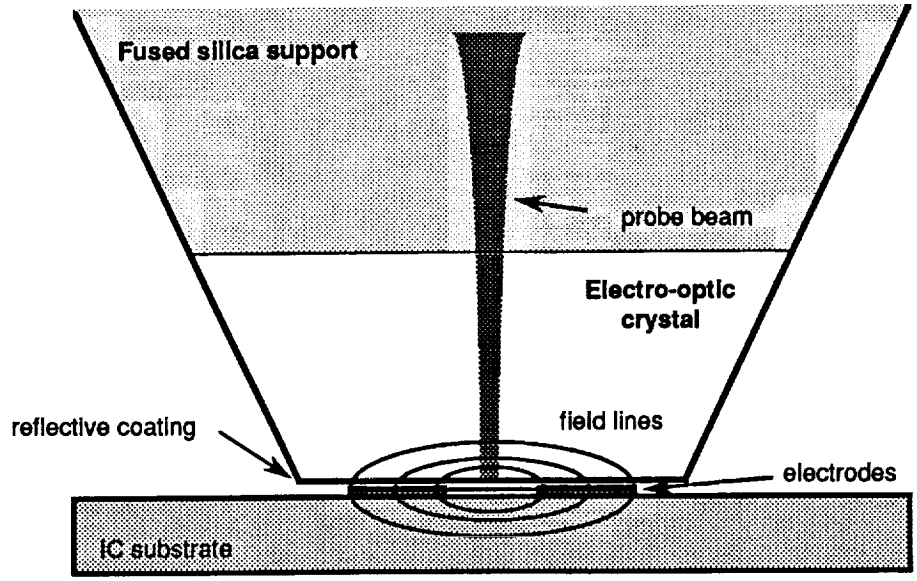
Fused silica support
probe beam
Electro-optic
crystal
reflective coating
field lines
electrodes
IC substrate

Fig. 2(b)

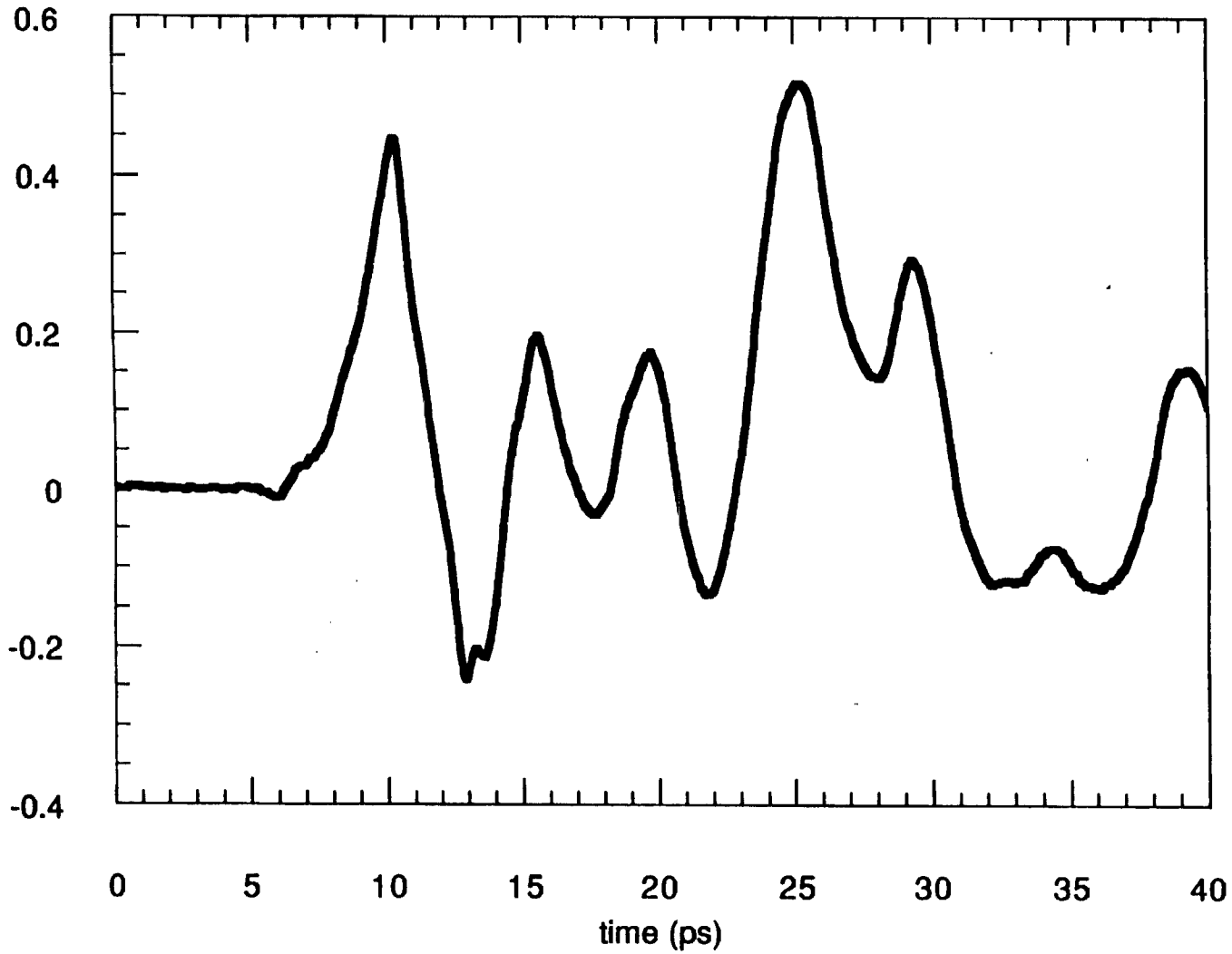

Fig. 3

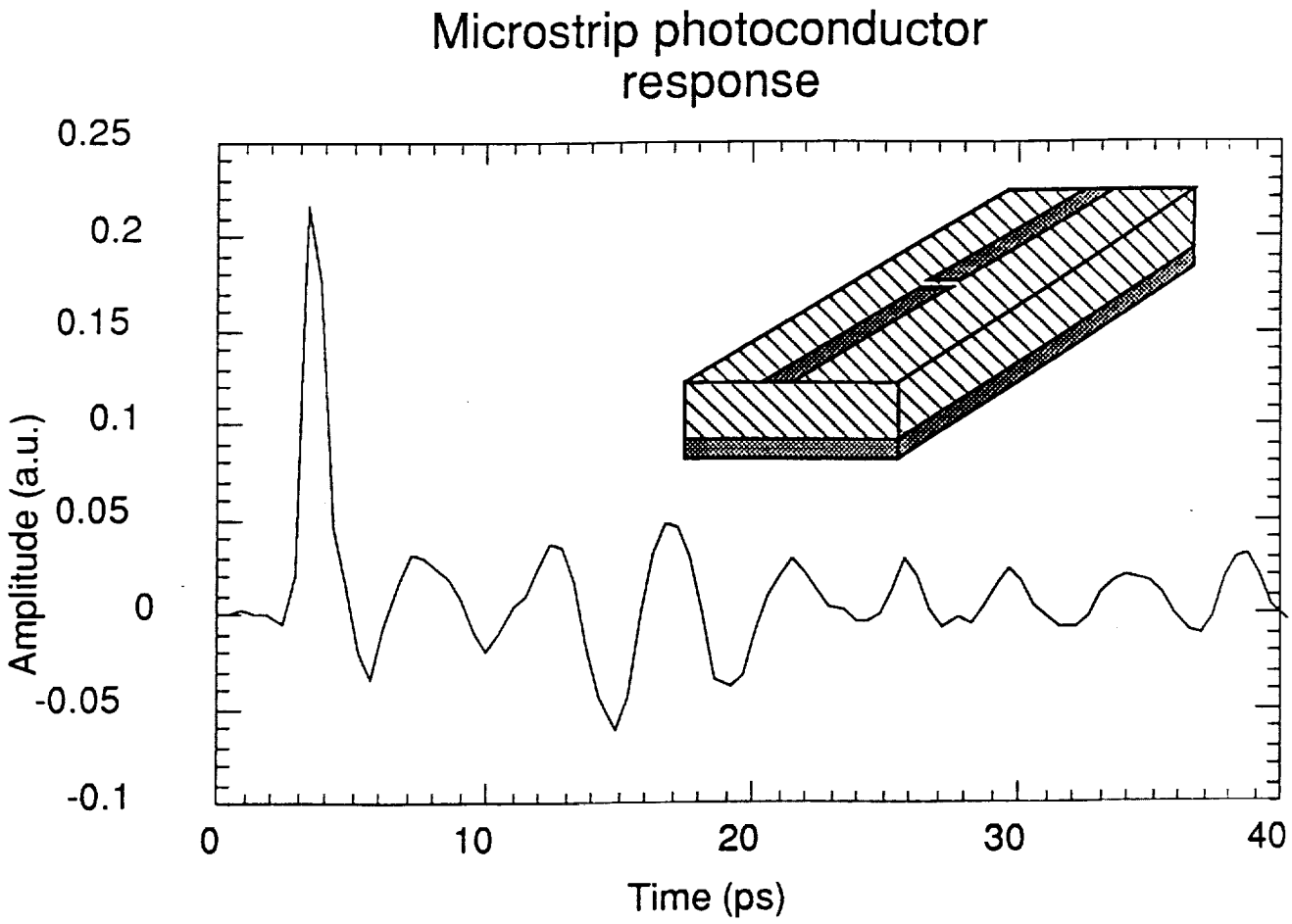
Microstrip photoconductor response
0.25
0.2
0.15
0.1
0.05
0
-0.05
-0.1
Amplitude (a.u.)
0
10
20
30
40
Time (ps)

Fig. 4

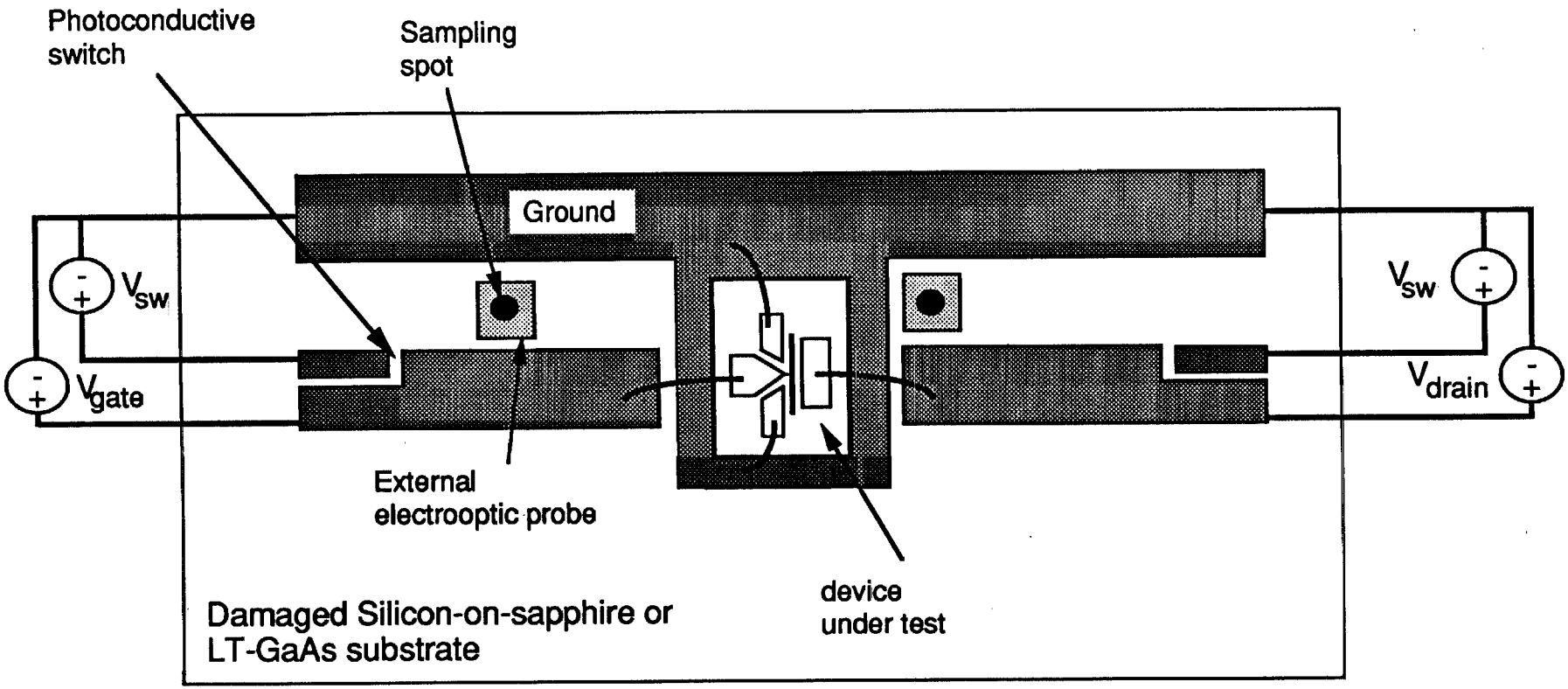
Photoconductive switch
Sampling spot
Ground
V_{sw}
V_{gate}
V_{sw}
V_{drain}
External electrooptic probe
device under test
Damaged Silicon-on-sapphire or LT-GaAs substrate

Fig. 5

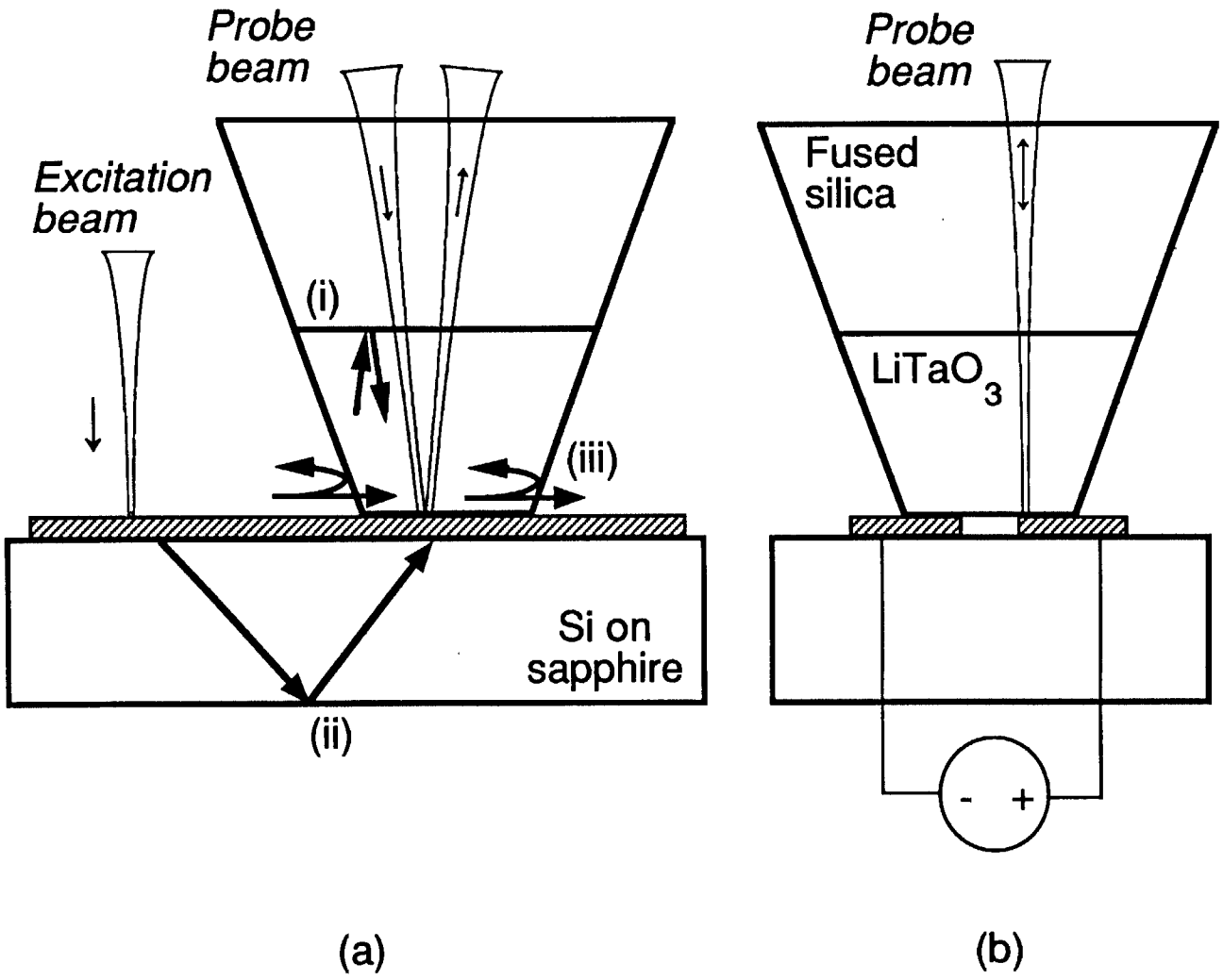
Probe beam
Excitation beam
(i)
(iii)
Si on sapphire
(ii)
(a)
Probe beam
Fused silica
LiTaO3
- +
(b)

Fig. 6

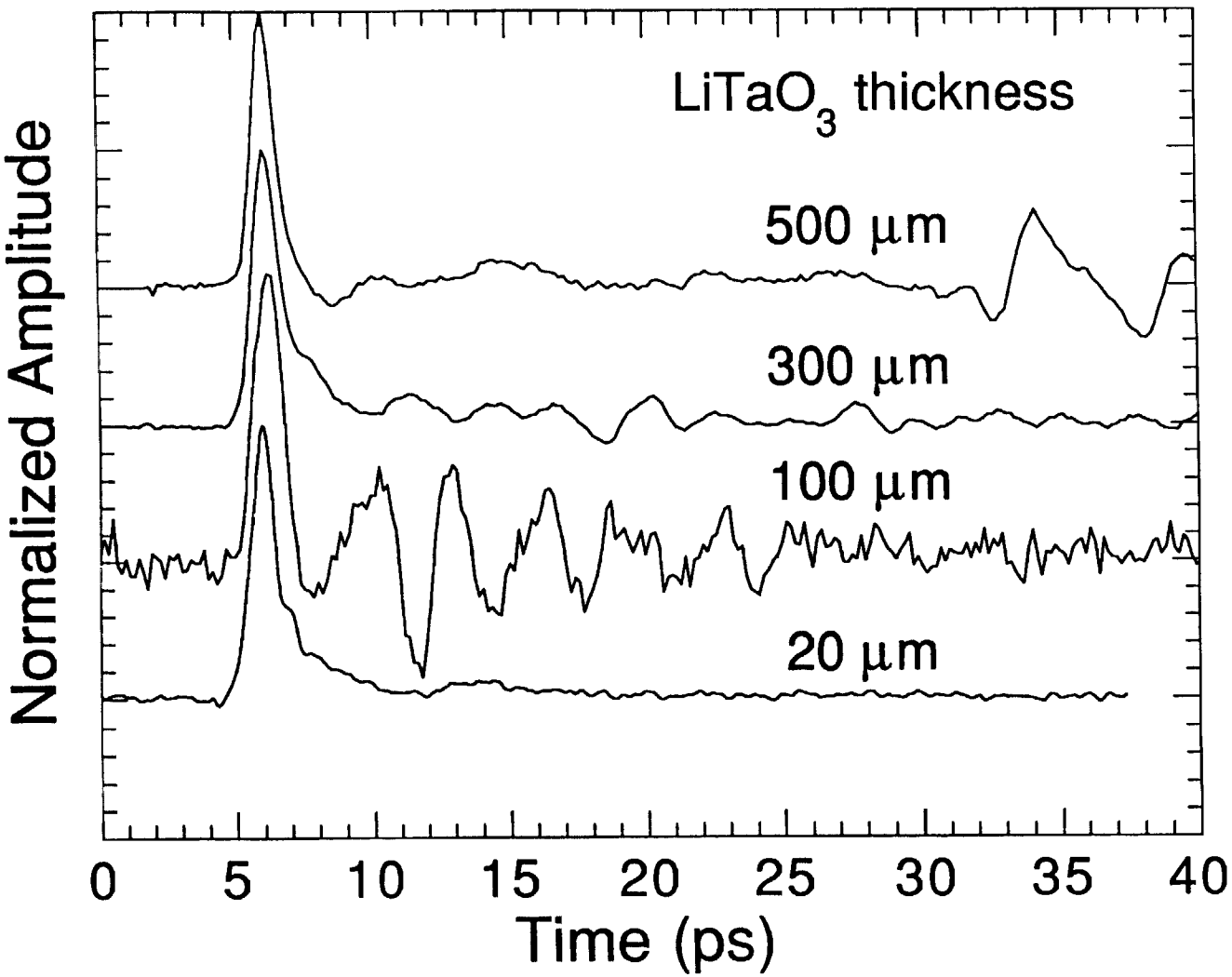
LiTaO3 thickness
500 μm
300 μm
100 μm
20 μm
Normalized Amplitude
0
5
10
15
20
25
30
35
40
Time (ps)

Fig. 7

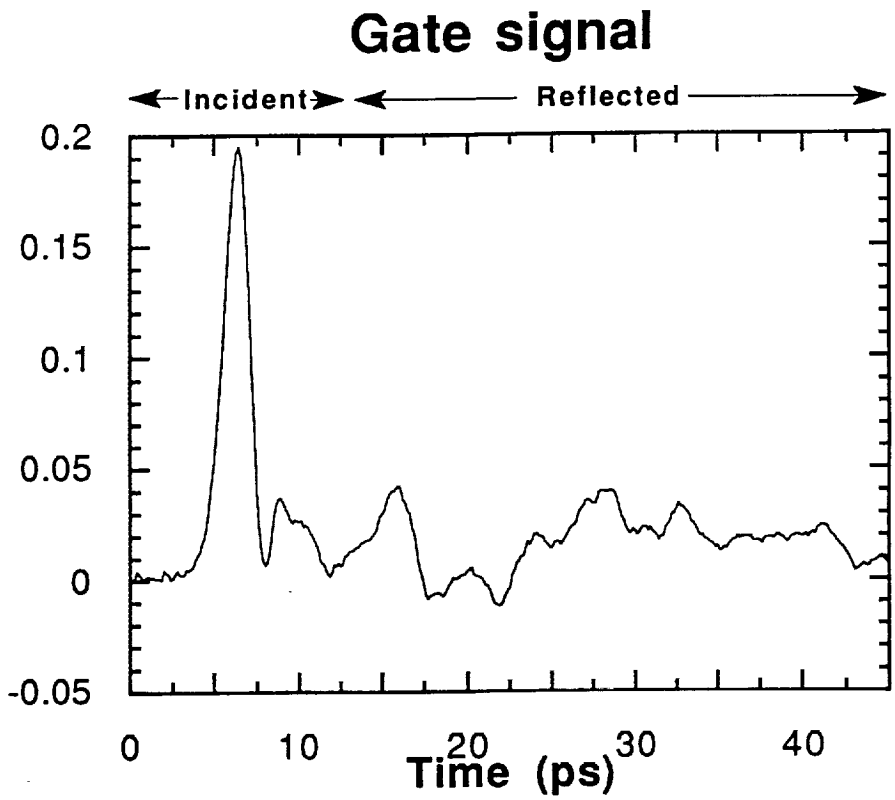
Gate signal
Incident
Reflected
0.2
0.15
0.1
0.05
0
-0.05
0
10
20
30
40
Time (ps)

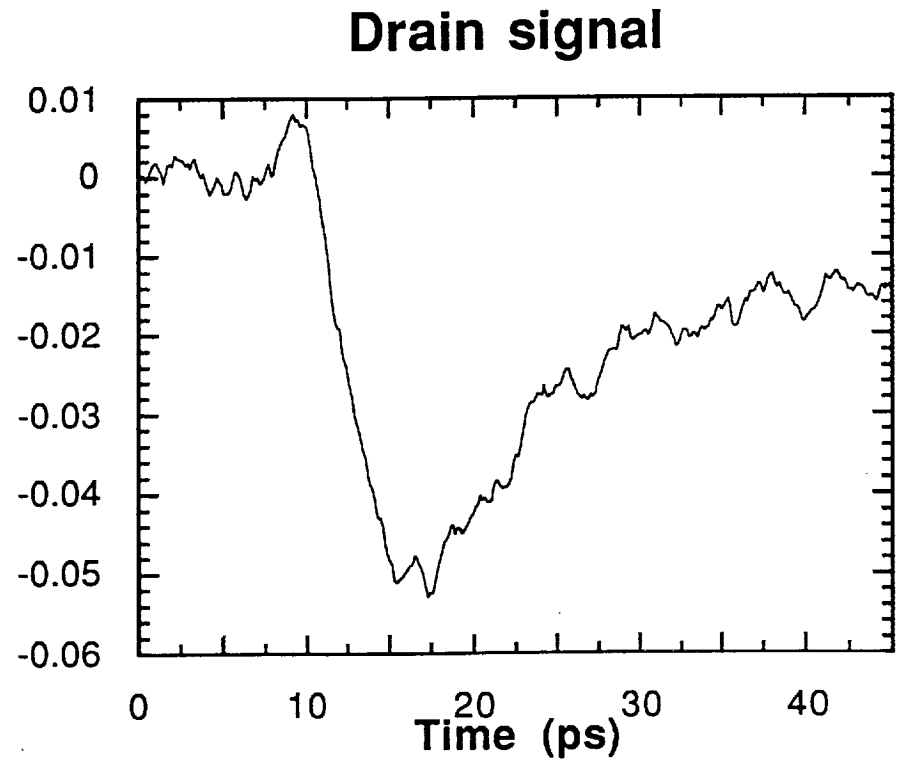
Drain signal
0.01
0
-0.01
-0.02
-0.03
-0.04
-0.05
-0.06
0
10
20
30
40
Time (ps)

Fig. 8

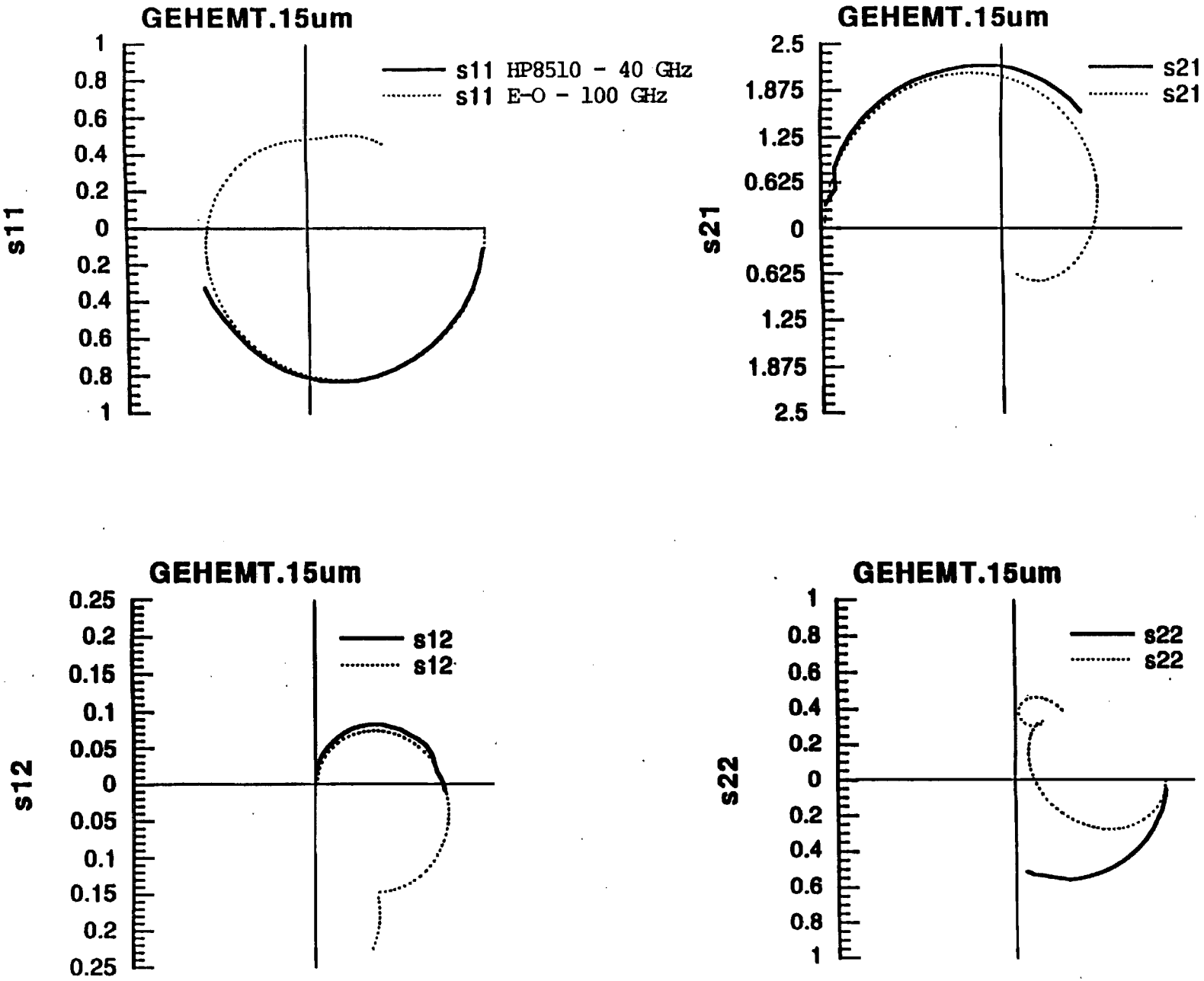
GEHEMT.15um
s11
1
0.8
0.6
0.4
0.2
0
0.2
0.4
0.6
0.8
1
s11 HP8510 - 40 GHz
s11 E-O - 100 GHz
GEHEMT.15um
s21
2.5
1.875
1.25
0.625
0
0.625
1.25
1.875
2.5
s21
s21
GEHEMT.15um
s12
0.25
0.2
0.15
0.1
0.05
0
0.05
0.1
0.15
0.2
0.25
s12
s12
GEHEMT.15um
s22
1
0.8
0.6
0.4
0.2
0
0.2
0.4
0.6
0.8
1
s22
s22

Fig. 9

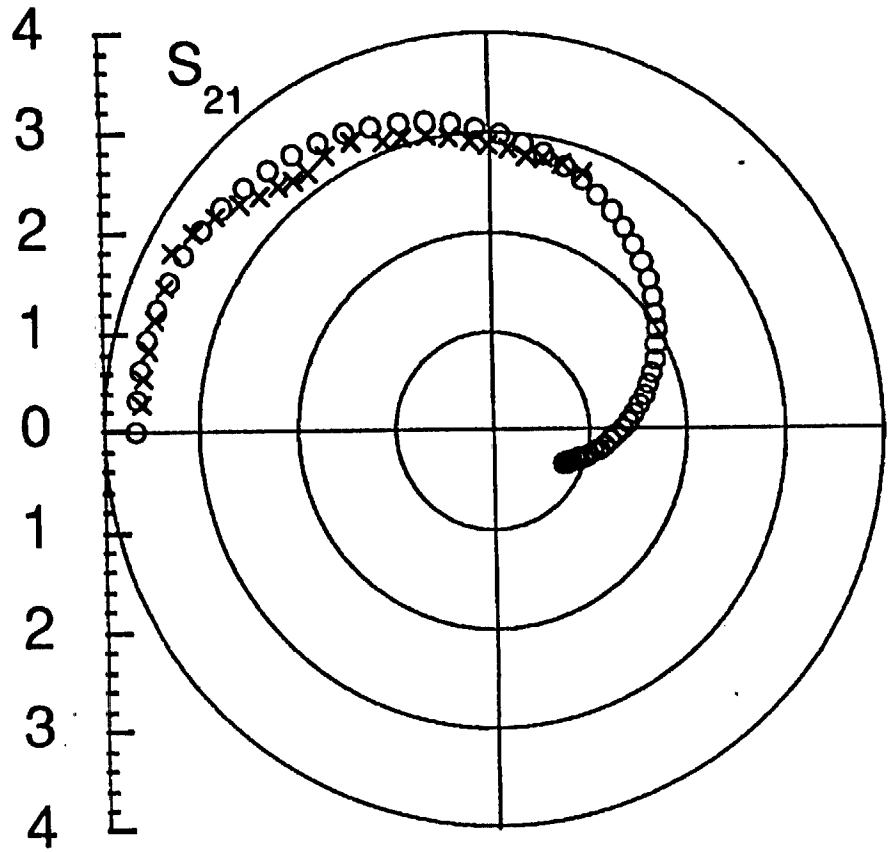

X - HP8510 data to 40 GHz
O - E-O data to 100 GHz

Fig. 10

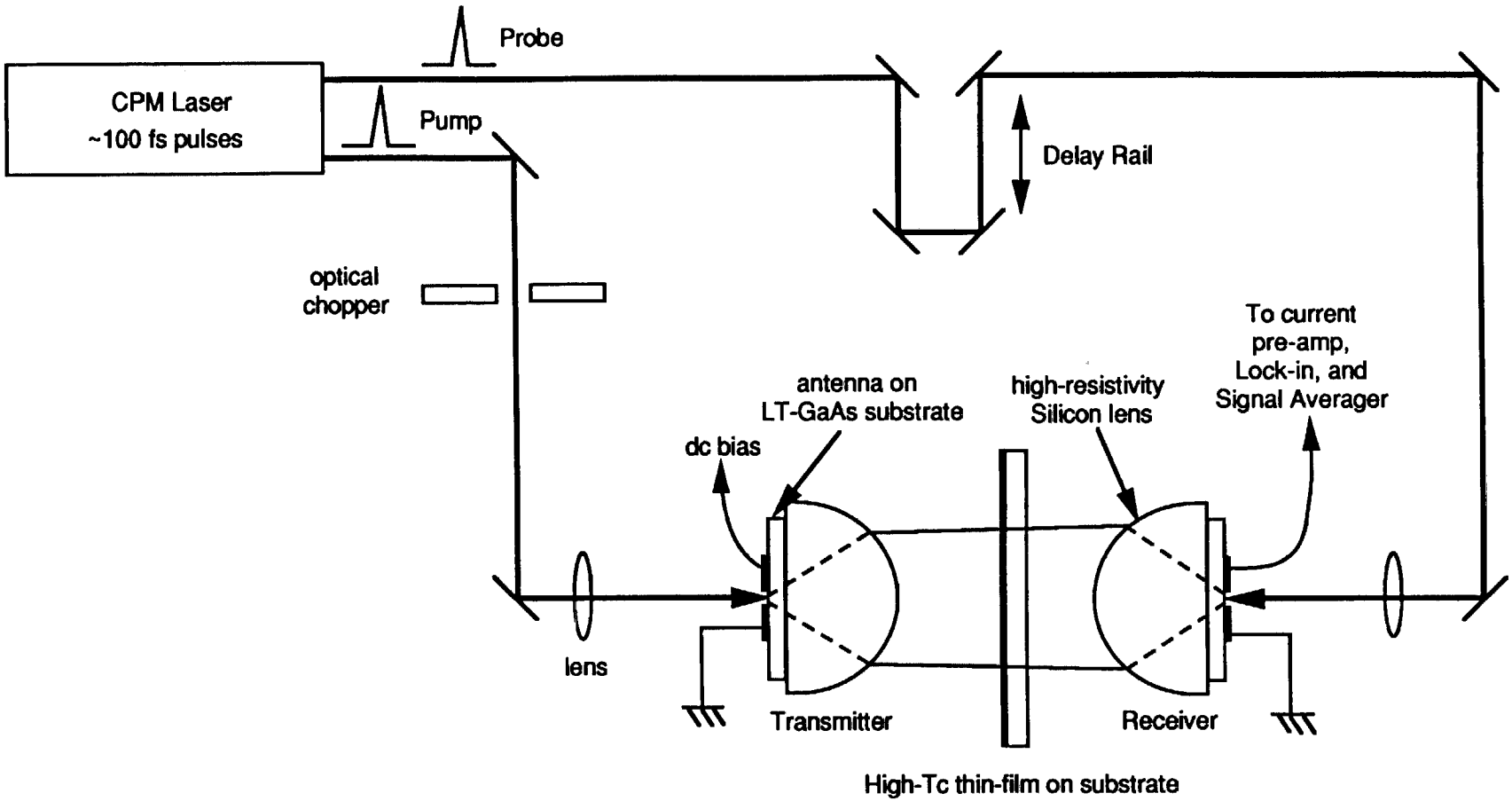
Probe
CPM Laser
~100 fs pulses
Pump
Delay Rail
optical
chopper
To current
pre-amp,
Lock-in, and
Signal Averager
antenna on
LT-GaAs substrate
high-resistivity
Silicon lens
dc bias
lens
Transmitter
Receiver
High-Tc thin-film on substrate

Fig. 11

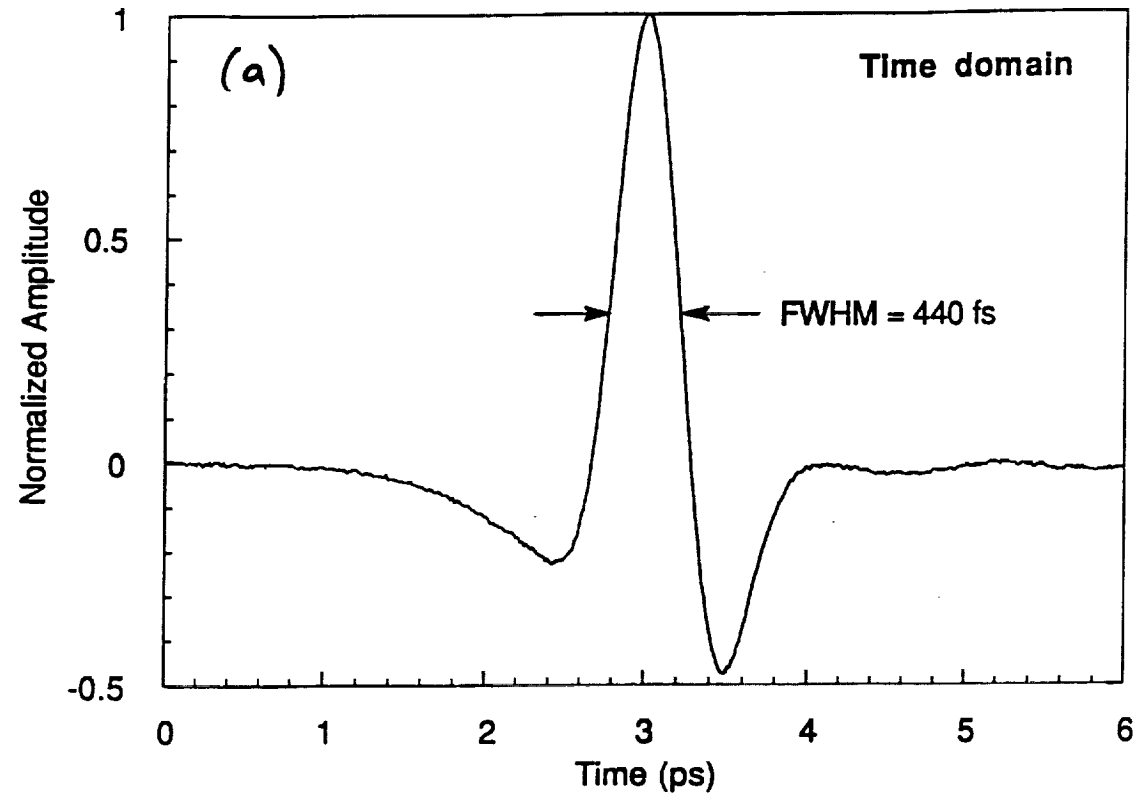
(a)
Time domain
FWHM = 440 fs
Normalized Amplitude
1
0.5
0
-0.5
0
1
2
3
4
5
6
Time (ps)

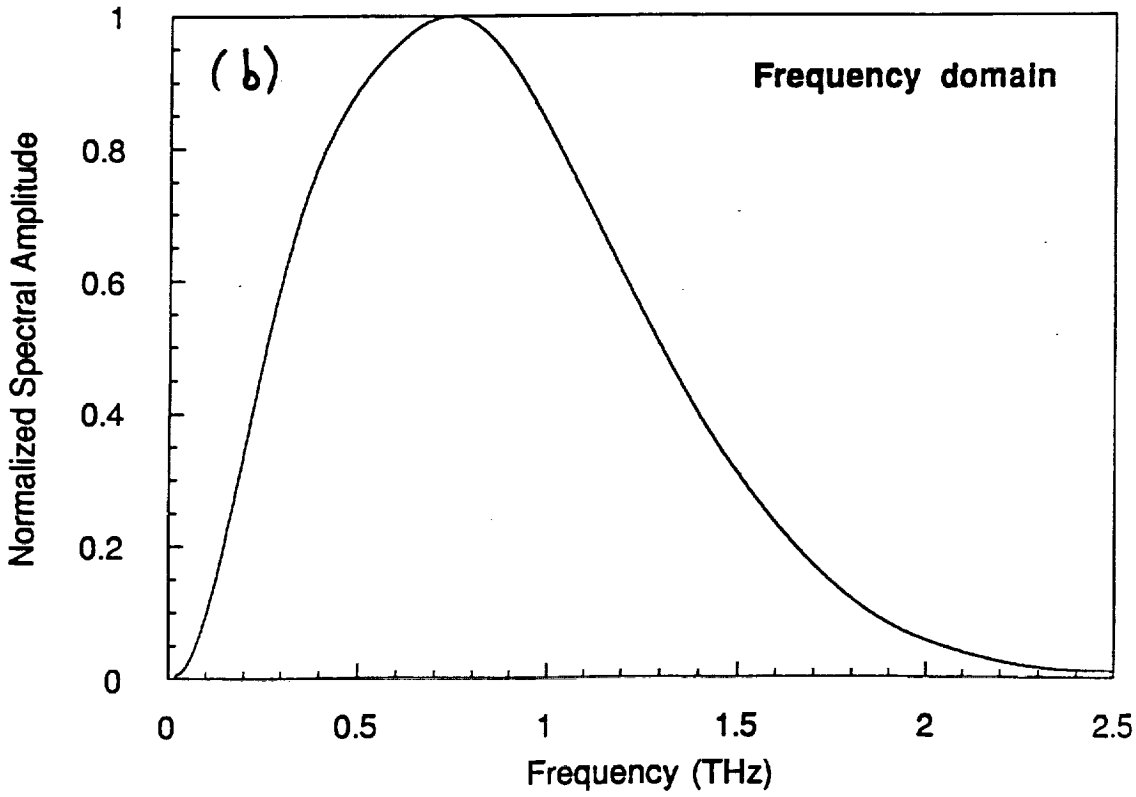
(b)
Frequency domain
Normalized Spectral Amplitude
1
0.8
0.6
0.4
0.2
0
0
0.5
1
1.5
2
2.5
Frequency (THz)

Fig. 12

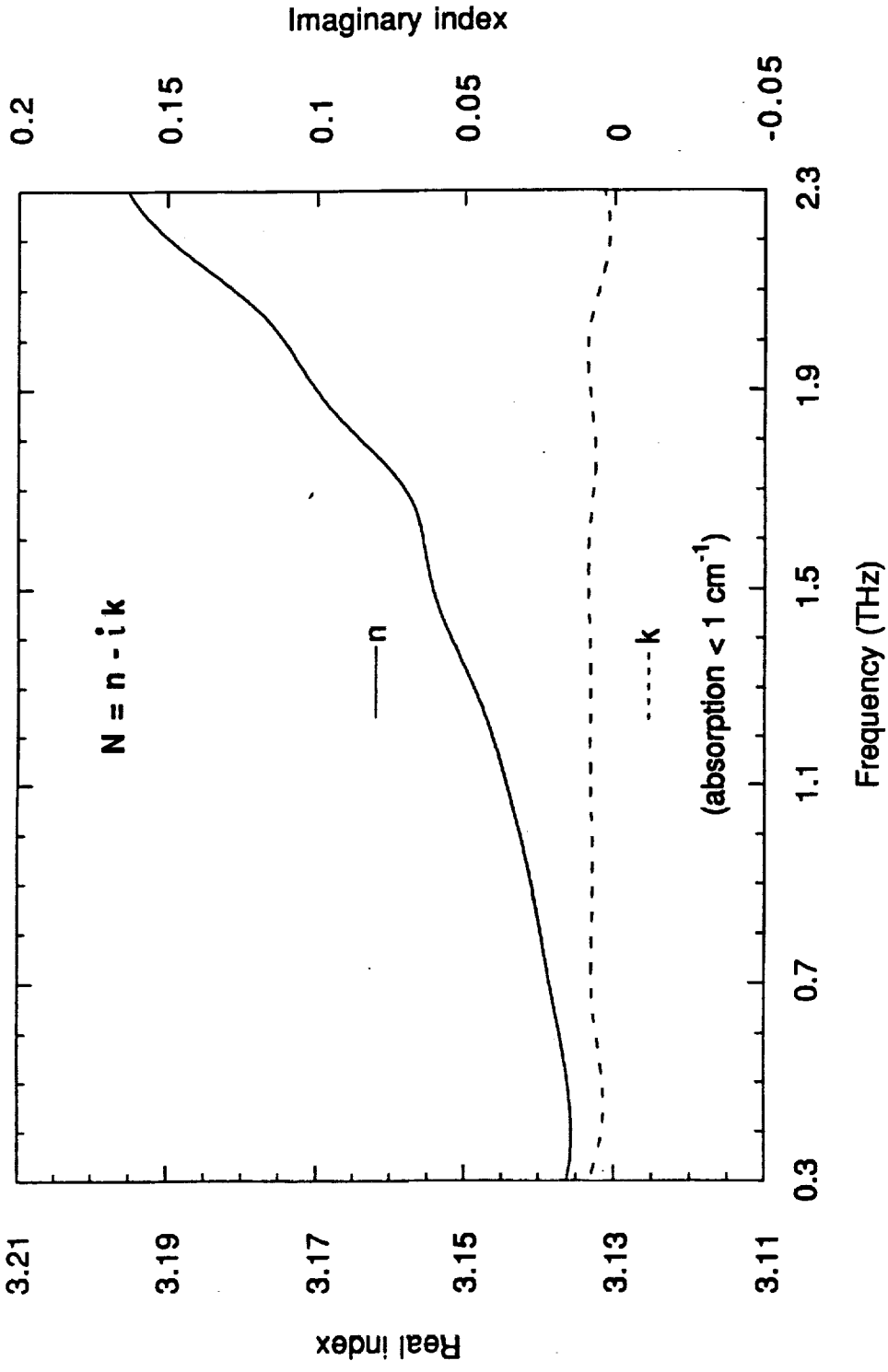
Imaginary index
0.2
0.15
0.1
0.05
0
-0.05
N = n - i k
n
k
(absorption < 1 cm-1)
0.3
0.7
1.1
1.5
1.9
2.3
Frequency (THz)
Real index
3.21
3.19
3.17
3.15
3.13
3.11

Fig. 13

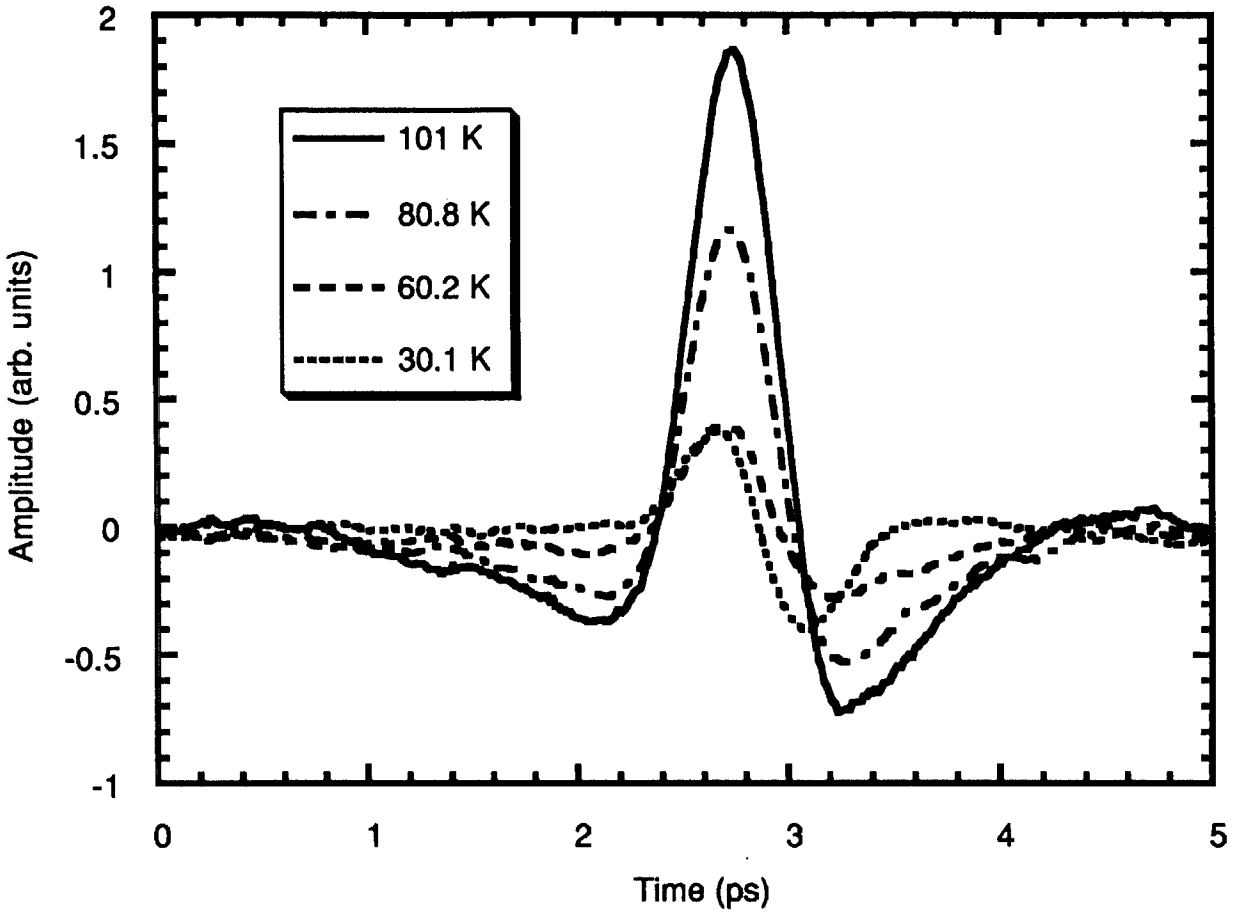
101 K
80.8 K
60.2 K
30.1 K
Amplitude (arb. units)
Time (ps)
2
1.5
1
0.5
0
-0.5
-1
0
1
2
3
4
5

Fig. 14

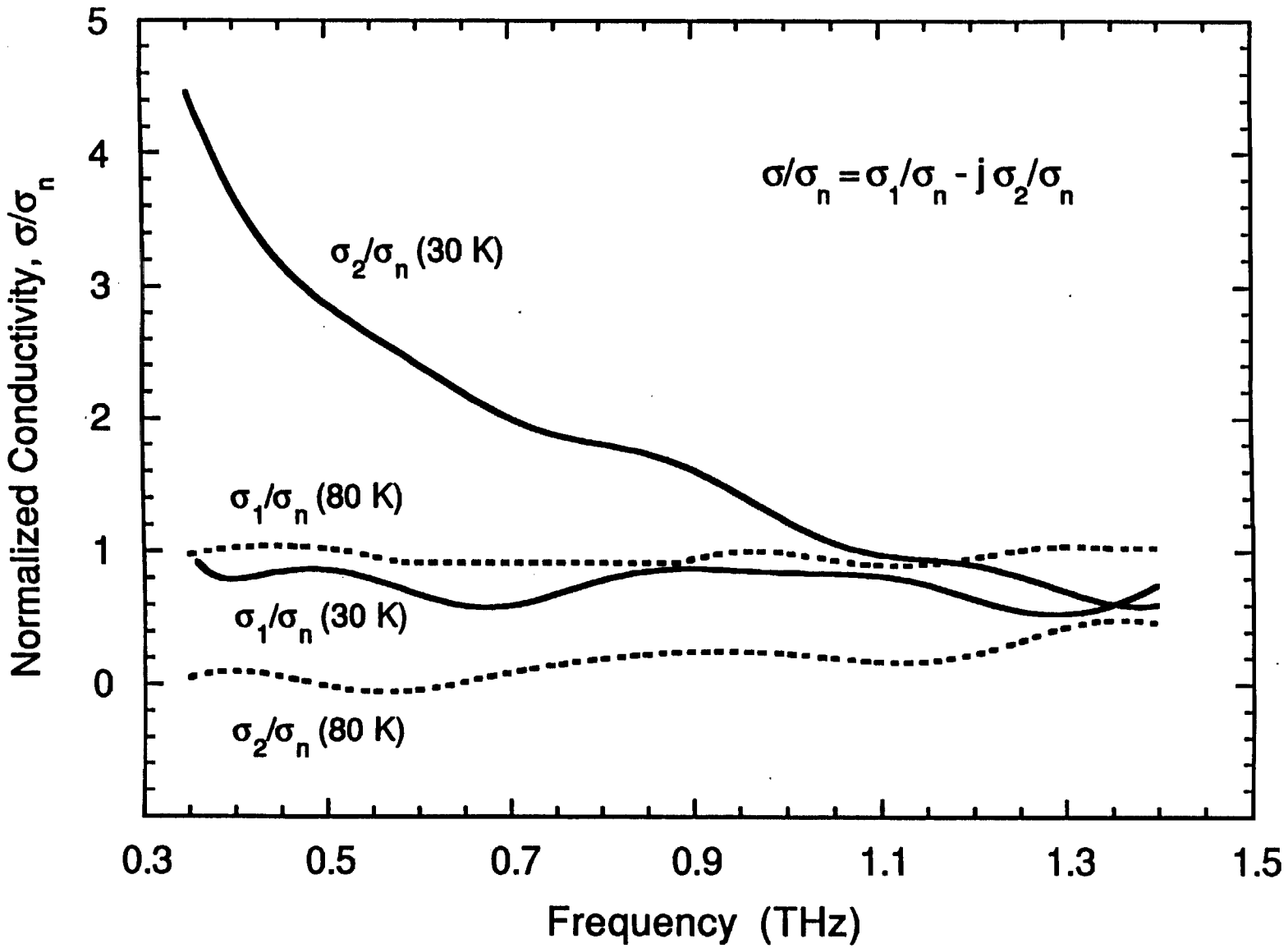
Normalized Conductivity, σ/σn
5
4
3
2
1
0
σ/σn = σ1/σn - j σ2/σn
σ2/σn (30 K)
σ1/σn (80 K)
σ1/σn (30 K)
σ2/σn (80 K)
0.3
0.5
0.7
0.9
1.1
1.3
1.5
Frequency (THz)

Fig. 15